Biomaterials Translational

Ångstrom-scale silver particle-infused hydrogels eliminate orthopedic implant infections and support fracture healing

Wei Du[1,2,3,4#], Jiang-Shan Gong[1,2#], Xia Chen[1,2,4,5], Yang Wu[1,2], Yu Yang[1,2], Sheng Zhu[1,2,4], Yu Zhang[1], Bei Chen[1], Yi-Wei Liu[1,2], Ze-Hui He[1,2], Zhe Guan[1,2], Yan Zhang[2,6,], Zhen-Xing Wang[1,2,4,*], Hui Xie[1,2,4,*]*

Key Words:
Ångstrom-scale silver particles; antibacterial; fracture healing; orthopedic implant infections; polyethylene glycol hydrogel

From the Contents

Introduction	85
Methods	86
Results	89
Discussion	97
Conclusion	99

ABSTRACT

Orthopedic implant-associated infections pose a significant clinical challenge, often requiring surgical intervention along with systemic antibiotic treatments. To address this issue, we developed a novel approach using Ångstrom-scale silver particles (AgÅPs) with broad-spectrum antibacterial properties. Specifically, we formulated a polyethylene glycol hydrogel infused with AgÅPs (Gel-AgÅPs) designed for treating fracture fixation infections. This novel hydrogel formulation is injectable, ensuring precise adherence to both the exposed tissue and fracture surfaces, thereby allowing the direct targeted action of AgÅPs at the infection site. The Gel-AgÅPs significantly reduced the infection caused by Escherichia coli (a model pathogen of orthopedic implant infection) in a murine femoral fracture model. Moreover, the Gel-AgÅPs-treated infected fractures healed completely within 6 weeks, exhibiting bone formation and mechanical strength comparable to those of uninfected fractures. Further analysis revealed a significant downregulation of local inflammatory response as evidenced by a lower expression of inflammatory markers in Gel-AgÅPs-treated fractures compared to untreated infected controls. Furthermore, Gel-AgÅPs exhibited a unique ability to inhibit osteoclast differentiation, a critical factor in infection-induced bone degradation, without impacting osteoblast activity. In conclusion, Gel-AgÅPs exerted a dual therapeutic effect by eradicating bacterial infection and mitigating inflammation-induced osteoclast activity, thereby expediting infected fracture healing. This innovative approach is a promising therapeutic alternative to conventional antibiotic treatments, potentially transforming the treatment landscape for orthopedic implant-associated infections.

#Authors contributed equally.

***Corresponding authors:**
Yan Zhang,
yanzhangcsu@csu.edu.cn;
Zhen-Xing Wang,
wangzx@csu.edu.cn;
Hui Xie,
huixie@csu.edu.cn

http://doi.org/10.12336/biomatertransl.2025.01.007

How to cite this article:
Du, W.; Gong, J.; Chen, X.; Wu, Y.; Yang, Y.; Zhu, S.; Zhang, Y.; Chen, B.; Liu, Y.; He, Z.; Guan, Z.; Zhang, Y.; Wang, Z.; Xie, H. Ångstrom-scale silver particle-infused hydrogels eliminate orthopedic implant infections and support fracture healing. *Biomater Transl.* **2025**, 6(1), 85-102.

Introduction

A substantial portion of clinical healthcare efforts and resources is devoted to treating orthopedic illnesses and injuries, which often require the utilization of biological implants and devices for effective management. However, the widespread use of internal fixations has led to increased post-operative infections, imposing a huge clinical and healthcare resource challenge in modern orthopedics. Following orthopedic surgeries, infection rates, especially those associated with fracture fixations, can vary significantly, ranging from 1 to 2% to over 30% in closed and open fractures, respectively.[1] These infections could lead to complications, such as fracture non-union, increased need for additional surgeries, prolonged hospital stays, and adversely impaired limb function recovery. Furthermore,

these complications could cause disability in severe cases or amputation, imposing profound economic and emotional burdens on both patients and their families.[2]

Orthopedic implant infections primarily occur through direct implant contamination, proximal infection dissemination, and transient bacteremia leading to implant colonization.[3] In addition to their limited efficacy, conventional therapeutic strategies, which mainly involve surgical debridement along with implant removal and prolonged systemic antibiotic therapy, are also expensive.[4-7] Furthermore, the rising threat of antibiotic-resistant bacteria is rapidly transitioning the medical landscape to a post-antibiotic era, rendering traditional treatment modalities increasingly ineffective.[8, 9]

This growing crisis has shifted research focus toward exploring alternative strategies, particularly in the field of nanotechnology. Nanoparticles, due to their unique properties, such as their ultra-small size, high surface reactivity, and substantial surface area-to-volume ratio, hold significant promise as agents for combating bacterial infections and circumventing antibiotic resistance.[10, 11] An example is silver nanoparticles that possess potent antibacterial, anti-inflammatory, and anticancer properties, making them useful in food and medical industries.[12, 13]

In our recent study, we developed Ångstrom-scale (0.1 nm) silver particles (AgÅPs) with an automated evaporation-condensation system designed by ourselves.[14] In addition to avoiding the risks and biological hazards associated with conventional methods, this innovative approach demonstrated efficacy in preventing bacterial colonization, reducing inflammation, and accelerating wound healing in diabetic and burn injuries animal models.[15] In addition, our previous investigations revealed that intravenous administration of AgÅPs can considerably reduce systemic bacterial load and enhance survival rates in septic mice.[16] However, the local treatment of fracture fixation-related infections using AgÅPs is yet to be explored.

Therefore, the present study introduces an AgÅPs-infused injectable hydrogel system that is specifically designed for the local treatment of orthopedic implant-related infections and fracture healing facilitation. For rapid crosslinking, the system uses a four-arm polyethylene glycol (PEG) with terminal maleimide groups (PEG-4ARM-Mal) and PEG-dithiol, yielding a porous and stable polymer network that is optimized for AgÅPs loading.[17] Our findings in a mouse femoral fracture infection model conclusively established that PEG hydrogel infused with AgÅPs (Gel-AgÅPs) can effectively eradicate bacterial colonization, alleviate inflammation-induced osteoclast differentiation, and accelerate infected fracture healing. Based on these findings, this study presents a groundbreaking alternative for orthopedic infection management and fracture treatment.

Methods

Preparation of Ångstrom-scale silver particles (AgÅPs) and PEG hydrogel infused with AgÅPs

In our previous research,[14, 18, 19] we detailed a method for synthesizing silver particles using a proprietary automated evaporation-condensation apparatus. Initially, the system was purged of air with a vacuum pump to ensure a clean environment. Subsequently, argon, an inert protective gas, was introduced and circulated within the system at a controlled pressure of 1×10^5–1×10^6 Pa, maintained by a gas blower. A continuous feed system delivered pure silver wire, measuring 8–12 cm in length and 0.1–0.8 mm in diameter, into the reaction chamber. Upon contact with a high-voltage electrode (25–45 kV), an arc discharge was triggered, vaporizing the silver wire into a gaseous state. This silver vapor, carried by the argon gas, was directed into a cooling chamber set at 0–4°C, where nucleation and particle growth occurred through coagulation, resulting in silver particles ranging from Ångstrom to nanoscale dimensions.

To prevent agglomeration, the newly formed silver particles underwent ultrasonic treatment at 15 kW and 15 kHz using a high-power ultrasonic dispersing unit. In addition, a demagnetization process was conducted using a current of 1,000 mA, a voltage range of 24–36 V, and a frequency of 23 Hz, enhancing particle separation. The processed silver particles were then directed to a particle segregation system equipped with three sequential collectors. By controlling the gas flow rate at 1.2 m/s, the particles were separated by sedimentation velocity into three distinct size categories: larger Ångstrom particles (>200 Å), intermediate Ångstrom particles (50–200 Å), and smaller Ångstrom particles (diameters spanning <50 Å) into their respective collectors. The focus of our study was on the smaller Ångstrom particles with diameters <50 Å.

The PEG-4ARM-Mal (20 kDa, Cat no: JKA7029) and PEG-dithiol (3.5 kDa, Cat no: JKA4001) were obtained from JenKem Technology (China). To synthesize Gel-AgÅPs, PEG-4ARM-Mal was first dissolved in an AgÅPs solution of approximately 500 ng/μL, following the methodology established in our previous work.[17] Concurrently, PEG-dithiol was dissolved in phosphate-buffered saline (PBS). The two solutions were then combined using the appropriate stoichiometric ratio to initiate hydrogel formation. For the preparation of the blank gel (Gel-blank), PEG-4ARM-Mal and PEG-dithiol were dissolved in PBS (pH 7.4) at a thiol-to-maleimide ratio of 2:1. Under basic conditions, a Michael addition reaction facilitated the formation of stable covalent bonds between thiolate groups and maleimide alkenes. This reaction resulted in the rapid formation of hydrogels within approximately 15 s.

[1]Department of Orthopaedics, Movement System Injury and Repair Research Centre, Xiangya Hospital, Central South University, Changsha, Hunan, China; [2]Hunan Key Laboratory of Angmedicine, Changsha, Hunan, China; [3]Department of Rehabilitation, Xiangya Hospital, Central South University, Changsha, Hunan, China; [4]National Clinical Research Centre for Geriatric Disorders (Xiangya Hospital), Changsha, Hunan, China; [5]Department of Clinical Laboratory, Xiangya Hospital, Central South University, Changsha, Hunan, China; [6]State Key Laboratory of Powder Metallurgy Central South University, Changsha, Hunan, China

Characterization of AgÅPs and PEG hydrogel infused with AgÅPs

The morphologies of AgÅPs were tested using a transmission electron microscope (JEM2100, JEOL LTD., Japan), and the size distribution of these nanoparticles was measured through image J software. The surface morphologies of both Gel-blank and Gel-AgÅPs were examined using a scanning electron microscope (SEM) (TESCAN MIRA, TESCAN, Czech Republic) under an accelerating voltage of 5 kV, followed by energy-dispersive spectroscopy (EDS) analysis to assess their elemental constitutions. Fourier-transform infrared spectra of the hydrogels were measured with a Nicolet iS5 Fourier transform infrared spectrometer (Thermo Fisher Scientific, United States) to analyze the chemical composition. Thermogravimetric analysis of the hydrogels was examined using a Q500 thermogravimetric analyzer (TA Instruments, United States) at a heating rate of 20°C/min from 30°C to 800°C to assess thermal stability. The hydrogels were subjected to amplitude and frequency sweep tests with a DHR-2 rheometer (TA Instruments, United States). Frequency sweeps were conducted at a constant strain of 1% from 0.1 to 5 Hz, and strain amplitude sweeps were performed at a constant frequency of 1 Hz, with amplitude ranging from 0.1 to 100%.

Bacterial strains and culture

The Department of Clinical Laboratory at Xiangya Hospital of Central South University provided bacterial strains of *Escherichia coli* ATCC15224, *Staphylococcus aureus* ATCC29213, and *Pseudomonas aeruginosa* ATCC27853. The bacteria were incubated in nutrient broth (GH6000, Taisite Tianjin Instrument Co., Ltd., China) at 37°C in a shaking incubator until reaching the mid-logarithmic phase for experimental use.

Cell culture

Eight-week-old C57BL/6 mice were used to obtain femurs and tibias tissues for isolating Sca-1$^+$CD29$^+$CD45$^-$CD11b$^-$ bone marrow-derived stem cells (BMSCs). Following euthanasia, bones were aseptically harvested, and BMSCs were isolated using flow cytometry (BD FACSAria III, BD Biosciences, United States). The BMSCs were cultured in alpha modification of Minimum Essential Medium Eagle (Cat no.: C3060-0500, XP Biomed, China) supplemented with 10% fetal bovine serum (FBS) (Cat no.: C04001-500, XP Biomed, China) and 1% penicillin-streptomycin (P/S) (Cat no.: P1400, Solarbio, China). The mouse monocyte/macrophage cell line RAW264.7 was purchased from Procell (Cat no.: CL-0190, China) and cultured in high-glucose Dulbecco's Modified Eagle Medium (DMEM) (Cat no.: C3110-0500, XP Biomed, China) supplemented with 10% FBS and 1% P/S. The cells were maintained in a humidified incubator at 37°C with 5% carbon dioxide.

Bacterial colony counting assay

To evaluate the antibacterial efficacy of Gel-AgÅPs, the bacteria (5×10^6 CFU/mL) were treated with 250 μg/mL levofloxacin (LEV), Gel-blank, and Gel-AgÅPs (250 ng/μL of AgÅPs), alongside a control group without treatment. After incubation for 8 h at 37°C and shaking at 300 rpm, the bacterial suspensions were diluted 10,000-fold with Luria–Bertani (LB) broth (Hopebio, China). Subsequently, 200 μL of each diluted sample was spread evenly onto LB agar plates. Following a 12-h incubation at 37°C, bacterial colonies were quantified to evaluate the antibacterial properties of each treatment.

Alamar blue assay

An Alamar Blue assay was conducted to further assess the antibacterial activity of the cells. Bacterial cultures (8×10^4 CFU per well) were treated with LEV (250 μg/mL), Gel-blank, and Gel-AgÅPs in a 96-well plate, along with an untreated control group. Each well contained LB medium supplemented with 10 μL of Alamar Blue reagent (Cat no.: 40202ES60, Yeasen, China). After a 4-h incubation, fluorescence intensity was measured using a Varioskan LUX multimode reader (Thermo Fisher Scientific, United States) at 570 nm excitation and 600 nm emission. Bacteria viability (%) was evaluated by comparing the fluorescence intensity ratios of treated cells to control cells.

Biofilm destruction assay

Biofilm formation was assessed by placing bacterial cultures (2×10^7 CFU per well) into 12-well plates and diluting them with Roswell Park Memorial Institute Medium (RPMI) 1640 medium (Cat no.: C3010-0500, XP Biomed, China). After 12-h incubation at 37°C, the medium was replaced with fresh RPMI 1640 containing LEV (250 μg/mL), Gel-blank, or Gel-AgÅPs (250 ng/μL), along with a control group. Following a 6-h incubation, wells were washed thrice with saline to remove planktonic bacteria. Biofilms adhering to culture plates were stained with crystal violet (200 μL per well, cat no.: 60506ES60, Yeasen, China) for 15 min. After three washes, the stained biofilms were air-dried, and the bound crystal violet was solubilized in 95% ethanol. The optical density (OD) at 570 nm was measured in a 96-well plate using a Varioskan LUX multimode reader.

To assess the destruction of bacterial biofilm, bacteria cultures (1 mL, 2×10^7 CFU per well) were first grown in RPMI 1640 medium for 12 h, followed by an additional 72 h in fresh medium to form mature biofilms. These biofilms were then treated with LEV (500 μg/mL), Gel-blank, or Gel-AgÅPs (250 ng/μL) for 36 h alongside an untreated control group. As described above, crystal violet staining was used to determine whether residual biofilms existed.

Osteogenesis induction

A density of 2×10^5 primary BMSCs per well was used to seed in 48-well plates. For osteogenic differentiation, the culture medium of the experimental group was supplemented with osteogenic induction factor (10 nM dexamethasone, 5 mM β-glycerophosphate, and 50 μg/mL ascorbic acid). The medium was also supplemented with either Gel-blank or Gel-AgÅPs. The positive control group (PC) (solvent + induced medium) was cultured in the osteogenic medium without Gel. In contrast, the negative control group (NC) (solvent) received Eagle's Minimum Essential Medium without

osteogenic supplements. Each condition was replicated in three wells. After a 7-day induction, the mineralization of osteogenic differentiation was stained with 2% Alizarin Red S (Cat no.: G1038, Servicebio, China) at pH 4.2 and observed using an inverted microscope (DMI4000B, Leica, Germany). An alkaline phosphatase assay kit (Cat no.: P0321, Beyotime, China) was used to measure alkaline phosphatase activity in the supernatants.

Osteoclastogenesis induction

A density of 2×10^3 RAW264.7 cells per well was used to seed in 48-well plates. The medium of the experimental group was supplemented with 100 ng/mL of receptor activator of nuclear factor-κB ligand (Cat no.: AF-310-01, Thermo Fisher Scientific, United States) and either Gel-blank or Gel-AgÅPs. DMEM with and without receptor activators of nuclear factor-κB ligand were given to positive and negative control groups, respectively. Each group consisted of triplicates. After a 12-day induction, cells were fixed and stained using a tartrate-resistant acid phosphatase (TRAP) staining kit (Cat no.: G1050, Servicebio, China). Osteoclastogenesis, indicated by the formation of multinucleated (three or more nuclei) cells, was quantified under an inverted microscope.

Cell counting kit-8 assay

The BMSC and RAW264.7 cells were separately seeded into 96-well plates at 37°C for 24 h (5×10^3 cells, 100 μL per well). Then, cells were treated with different silver particles (0, 2, 4, 8, 16, 32 μg/mL). All culture medium was removed after 24 h of incubation, and then, the cells were cultured with 100 μL fresh complete medium containing 10 μL cell counting kit-8 reagent (CCK-8) (Yeasen, China) for 2 h. The microplate reader measured the absorbance per well at 450 nm.

Qualitative real-time polymerase chain reaction (qRT-PCR) analysis

Total RNA from cells in different treatment groups was extracted and processed for complementary DNA synthesis. Then, qRT-PCR was carried out using the FTC-3000 real-time PCR system (Funglyn Inc., Canada) with 2Inc.,-time PCR system (olymerSelleck, United States). Relative gene expressions were measured using the $2^{-\Delta\Delta CT}$ method with reference to *Gapdh*. Primer sequences for qRT-PCR were as follows:

(i). *Il1b* (mouse): Forward: 5'-GAAATGCCACCTTTTGACAGTG-3' and reverse: 5'-TGGATGCTCTCATCAGGACAG-3'.

(ii). *Il6* (mouse): Forward: 5'-TAGTCCTTCCTACCCCAATTTCC-3' and reverse: 5'-TTGGTCCTTAGCCACTCCTTC-3'.

(iii). *Tnfa* (mouse): Forward: 5'-TGAACTTCGGGGTGATCGGTC-3' and reverse: 5'-CACTTGGTGGTTTGCTACGACG-3'.

(iv). *Bglap* (mouse): Forward, 5'- TTCTGCTCACTCTGCTGACCC-3' and reverse: 5'-CTGATAGCTCGTCACAAGCAGG-3'.

(v). *Runx2* (mouse): Forward: 5'- CGCCACCACTCACTACCACAC-3 and reverse: 5'-TGGATTTAATAGCGTGCTGCC-3'.

(vi). *Alpl* (mouse): Forward: 5'- CCAACTCTTTTGTGCCAGAGA-3' and reverse: 5'-GGCTACATTGGTGTTGAGCTTTT-3'.

(vii). *Trap* (mouse): Forward: 5'-TGGTCCAGGAGCTTAACTGC-3' and reverse: 5'-GTCAGGAGTGGGAGCCATATG-3'.

(viii). *Mmp9* (mouse): Forward: 5'-CTGGACAGCCAGACACTAA AG-3' and reverse: 5'-CTCGCGGCAAGTCTTCAGAG-3'.

(ix). *Ctsk* (mouse): Forward: 5'-GAAGAAGACTCACCAGAAGCAG-3' and reverse: 5'-TCCAGGTTATGGGCAGAGATT-3'.

(x). *Gapdh* (mouse): Forward: 5'-CACCATGGAGAAGGCCGGGG-3' and reverse: 5'-GACGGACACATTGGGGGTAG-3'.

Murine femur fracture model

Animal care and experimental procedures were approved by the Ethics Review Committee of Xiangya Hospital of Central South University (approval number: 202101007) in accordance with the Guidelines for the Ethical Review of Laboratory Animal Welfare People's Republic of China National Standard GB/T 35892-2018. Eight-week-old C57BL/6 male mice (n = 85) were subjected to general anesthetization. A lateral skin incision was made over the right femur, followed by blunt dissection to expose the mid-femur. The intercondylar notch of the distal femoral bone was penetrated with a sterile 23-gauge needle and advanced along the medullary canal. A transverse fracture was created using micro-scissors to interrupt the femur. The needle was inserted into the femoral shaft in this model to stabilize a femoral fracture, and then, the fracture was treated with an *in situ* polymerized hydrogel. The injectable hydrogel formulation is designed to adhere efficiently to exposed tissue and fracture surfaces, ensuring localized therapeutic agent delivery. The mice were then randomly divided into three groups: Control (fracture only, n = 6), Gel-blank + *E. coli* (n = 8), and Gel-AgÅPs + *E. coli* (n = 7). Each fracture site received 20 μL of the corresponding intervention and 2 μL of *E. coli* solution (5×10^6 CFU/mL bacteria). After hydrogel polymerization at the fracture site, the incision was sutured. Post-operative monitoring included observation of general health and mobility. At 3- or 6-week post-treatment, the right femora of the mice were harvested and fixed in 4% paraformaldehyde for 24 h.

Micro-computed tomography (μCT) analysis

μCT scanning was performed using a vivaCT80 scanner (SCANCO Medical AG, Swiss) at 55 kV and 145 μA, with a resolution of 11.4 μm. The fracture callus was constructed in three dimensions and analyzed using NRecon (version 1.6.3.3), CTAn (version 1.11.0.0), and μCTVol (version 2.2.0.0) software. Approximately 700 slices around the fracture line were analyzed. The region of interest was defined to include the callus, and a consistent threshold was applied to differentiate mineralized tissue. Bone volume (BV), tissue volume (TV), and BV/TV ratio were quantified and analyzed.

Recovery of bacteria from tissue samples

After euthanasia, sterile cotton swabs were used to collect bacterial samples from the femur surface, stabilization needle, and surrounding muscle tissue. Swabs were placed in 1 mL PBS and incubated for 2 h at 37°C. The suspension was diluted 10,000-fold with LB broth, and 200 μL was spread on LB agar plates. A 12-h incubation at 37°C was followed by the counting of bacterial colonies using Image ProPlus (version 6.6.6.260).

In vivo bacteriostasis of PEG hydrogel infused with AgÅPs

Following the previously described surgical fracture model and treatment protocols, mice were randomly divided into five groups: Control (fracture only, n = 3), Gel-blank + *E. coli* (n = 3), LEV + *E. coli* (n = 3), AgÅPs + *E. coli* (n = 3), and Gel-AgÅPs + *E. coli* (n = 3). After a 7-day treatment period, bacteria were recovered from tissue samples using the method detailed in the recovery of bacteria from tissue samples section.

Histological and immunohistochemical analyses

After a 48-h fixation in 4% paraformaldehyde, the dissected femora were decalcified in 10% ethylenediaminetetraacetic acid (pH 7.4) at 4°C on a rocking platform for 7 days. After sequential dehydration in graded ethanol series, samples were embedded in paraffin. The bone samples were then cut into longitudinal sections of 5 μm thickness. Sagittal sections from the fracture areas were stained with hematoxylin and eosin (H/E) (Cat no.: GP1031, Servicebio, China), Safranin-O/Fast Green (SO/FG) (Cat no.: G1371, Solarbio, China), and tartrate-resistant acid phosphatase (Cat no.: G1050, Servicebio, China) for histological evaluation. Immunohistochemical staining was performed using primary antibodies against osteocalcin (OCN) (Cat no.: GB11233, Servicebio, China) with a dilution of 1:300, tumor necrosis factor-alpha (TNF-α) (Cat no.: GB11188, Servicebio, China) with a dilution of 1:800, and interleukin-1 beta (IL-1β) (Cat no.: GB11113, Servicebio, China) with a dilution of 1:400. Appropriate secondary antibodies (anti-rabbit, dilution 1:200) were applied for visualization.

Biomechanical testing

Three-point bending tests were performed on a computer-controlled machine (3343M1372, Instron, United States) to evaluate the biomechanical properties of the healed femora. A femur with its patellar surface facing upward was positioned anterior-posterior on the lower support struts 9 mm apart. An upper loading bar of 5.5 mm span was utilized. A constant vertical compressive load was applied at a speed of 3 mm/min until failure. Three millimeters per minute of continuous vertical compression was applied until failure. An automatic recorder was used to record maximum bending loads (N).

Multi-analyte flow assay

Serum levels of interferon-gamma (INF-γ), IL-2, IL-6, and TNF-α were quantified using LEGENDplex Multi-Analyte Flow Assay Kits (741050, Biolegend, United States). Assays were conducted following the manufacturer's instructions.

Statistical analysis

Data points from individual experiments are represented as dots, with lines indicating mean values and error bars denoting standard deviation. Statistical analyses were carried out using Student's *t*-test for two-group comparisons and one-way or two-way analysis of variance with Bonferroni's *post hoc* test for multiple-group comparisons. All statistical calculations were performed using GraphPad Prism version 9. A $p < 0.05$ was considered statistically significant. Figures are self-made using Adobe Illustrator 2023.

Results

Characterization of AgÅPs infused injectable four-arm PEG hydrogels

The AgÅPs-infused PEG hydrogels were formed using a PEG-4ARM-Mal and PEG-dithiol as the skeleton, followed by a subsequent introduction of AgÅPs in a doping process. Herein, AgÅPs synthesis followed a protocol established in our previous publication.[19] The Gel-AgÅPs were synthesized in a single step using a Michael addition reaction. Specifically, AgÅPs were dissolved in a PEG-dithiol-PEG-4ARM-Mal mixture, thereby preserving their activity during hydrogel synthesis. The resulting injectable formulation allows for a sustained AgÅPs release through passive diffusion in the hydrogel matrix. This targeted approach combats bacteria, aiding in bone regeneration and fracture healing (Figure 1A).

Transmission electron microscope image revealed that AgÅPs had a sphere shape with diameters of 3.54 ± 0.47 nm (Figure 1B and C). The gelation time was approximately 15 s (Figure 1D), implying the possibility of lowering the operative duration and infection risk during fracture fixation. Furthermore, SEM analysis revealed notable morphological changes in the hydrogel after integrating AgÅPs. The Gel-blank exhibited a smooth surface, which changed into a rough, uniformly distributed granular texture after adding AgÅPs, indicating that AgÅPs were successfully incorporated into the PEG matrix (Figure 1E). The chemical compositions of Gel-blank and Gel-AgÅPs were measured using EDS. The elemental silver was only detected in Gel-AgÅPs and not in Gel-blank (Figure 1F), further confirming it was successfully embedded into the hydrogel. To further evaluate the stability of AgÅPs in the hydrogel matrix, we performed SEM-EDS analysis on Gel-AgÅPs samples that had been placed for 1 and 2 weeks, respectively. The results showed that the relative rate and content of Ag in 1- and 2-week samples decreased only slightly compared to the initial measurement at 0 weeks, and this reduction could be considered reasonable (Figure 1G and H). This suggests that AgÅPs are relatively stable within the hydrogel matrix and are slowly released.

The chemical structure of the hydrogels was investigated with Fourier transform infrared spectroscopy. The spectra revealed similarities between the Gel-blank and Gel-AgÅPs groups, with absorption peaks ranging between 3,500 cm^{-1} and 3,250 cm^{-1}, indicating the amino group stretching vibrations. Notably, the analysis revealed the absence of double bond peaks near 3,100 cm^{-1}, confirming the successful completion of the reaction between PEG-4ARM-Mal and PEG-dithiol.

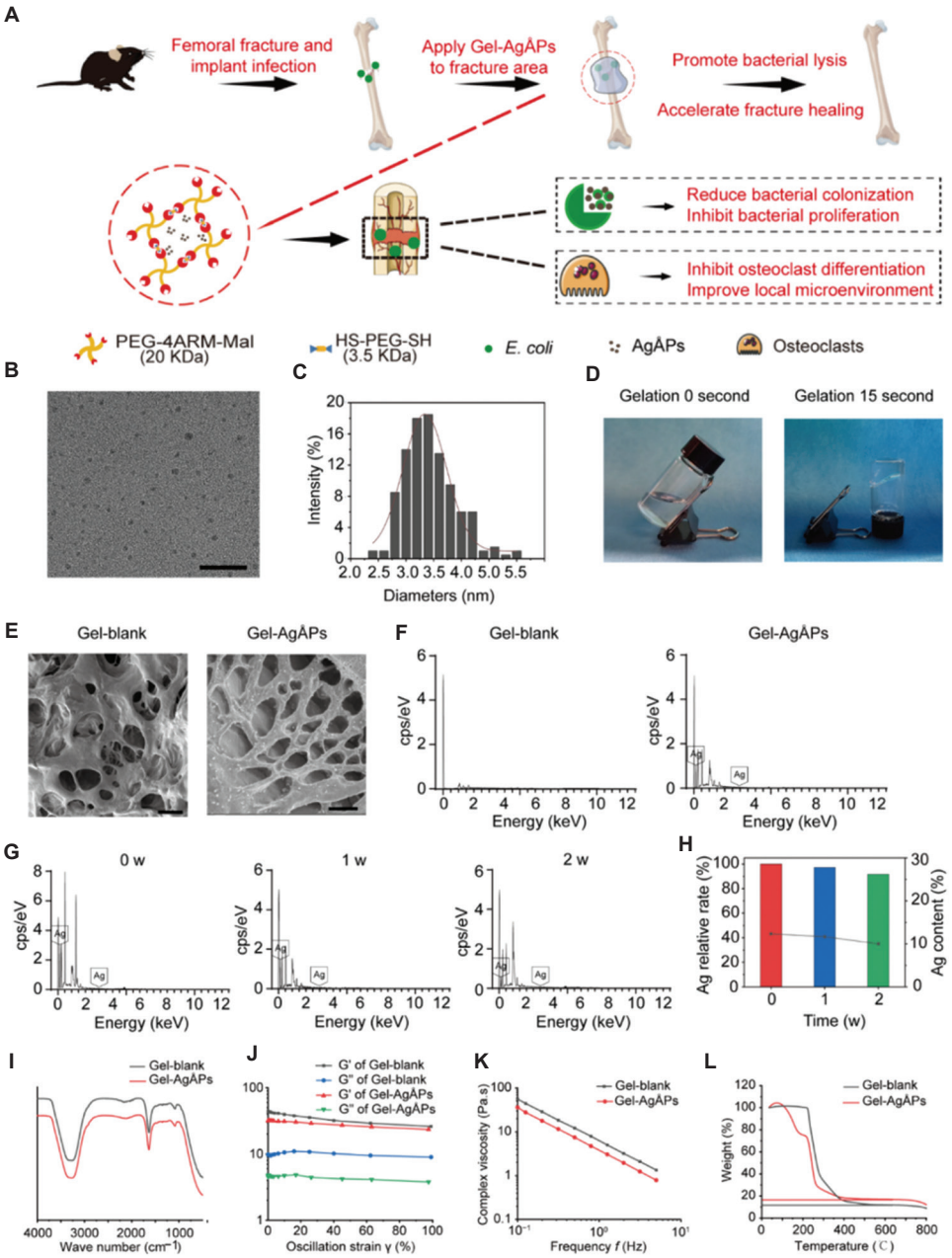

Figure 1. Characterization of AgÅPs infused injectable polyethylene glycol hydrogels. (A) Schematic representation of Gel-AgÅPs mechanism showing eradication of bacterial colonization, suppression of inflammation-induced osteoclast differentiation, and promotion of infected fracture healing. (B) TEM image of AgÅPs. Scale bar, 20 nm, magnification: 5000×. (C) Size distribution of AgÅPs (3.54 ± 0.47 nm, n = 200) calculated from TEM images. (D) Time-lapse images illustrating the rapid gelation process of Gel-AgÅPs within 15 s. (E) SEM images of the surface morphology of Gel-blank (left) and Gel-AgÅPs (right). Scale bar: 100 μm, magnification: 50×. (F) EDS spectra of blank-gel and Gel-AgÅPs. (G & H) EDS spectra of Gel-AgÅPs at different time points (G) and the trend of AgÅPs content variation (H). (I) FTIR spectra of Gel-blank and Gel-AgÅPs, highlighting their chemical compositions. Rheological properties of Gel-blank and Gel-AgÅPs assessed via amplitude (J) sweep test and (K) frequency sweep test. (L) Thermogravimetric analysis curves comparing the thermal stability of Gel-blank and Gel-AgÅPs. Abbreviations: Ag: Silver; AgÅPs: Ångstrom-scale silver particles; *E. coli: Escherichia coli*; EDS: Energy-dispersive spectroscopy; FTIR: Fourier transform infrared spectroscopy; Gel: Hydrogel; HS-PEG-SH: Polyethylene glycol-dithiol; PEG-4ARM-Mal: Four-arm polyethylene glycol; SEM: Scanning electron microscopy; TEM: Transmission electron microscopy.

Peaks ranging from 2,926 cm^{-1} to 2,852 cm^{-1} represented asymmetric and symmetric stretching vibrations of the methylene (CH_2) group, whereas a peak at 1,632 cm^{-1} was attributed to the amide carbonyl group. Furthermore, peaks at 1,463 cm^{-1} and 1,349 cm^{-1} corresponded to carbon-hydrogen bending and CH_2 wobbling, respectively. In addition, the peak at 1,080 cm^{-1} indicated the stretching of the carbonyl group in PEG (Figure 1I).[20] These findings show that AgÅPs addition did not induce structural changes in the hydrogel.

Rheological evaluations of Gel-AgÅPs revealed a significant viscoelastic solid behavior. As shown in the correlation scan analysis within the linear viscoelastic region, the storage modulus (G') was greater than the loss modulus (G") (Figure 1J).

The hydrogel exhibited shear thinning behavior after AgÅPs incorporation, indicating increased viscosity (Figure 1K).[21] Thermogravimetric analysis estimated AgÅPs loading in the hydrogel to be around 5%, with a notable enhancement in thermal stability post-AgÅPs doping, as evidenced by weight reduction trends observed in both the Gel-blank and Gel-AgÅPs groups up to 400°C (Figure 1L). These findings collectively suggest the successful synthesis of AgÅPs-infused hydrogels, laying the groundwork for subsequent investigations into their therapeutic efficacy.

Antibacterial efficacy of PEG hydrogel infused with AgÅPs against common bacteria

The Gel-AgÅPs were assessed for antibacterial efficacy against *S. aureus* (Gram-positive), *E. coli* (Gram-negative), and *P. aeruginosa* (Gram-negative), the three prevalent bacteria commonly implicated in orthopedic infection.[22] Recognizing their varied pathogenic profiles, strains of methicillin-sensitive *S. aureus*, *E. coli*, and *P. aeruginosa*, were employed to rigorously test the antibacterial activity of the Gel-AgÅPs hydrogel formulation. LEV, a well-known antibiotic, was included as a control to benchmark the antibacterial efficacy of Gel-AgÅPs.

Our experimental setup involved the synthesis of hydrogels containing bacterial cultures of *E. coli*, *S. aureus*, or *P. aeruginosa* entrapped within the hydrogel matrices, both with and without AgÅPs. Subsequently, we cultured the gels in bacterial growth media and tested them for viable bacteria after 24 h. According to the results, Gel-AgÅPs significantly reduced the bacterial count to very low levels across all tested strains (Figure 2A), highlighting their potent bactericidal capacity. As an additional way of assessing antimicrobial susceptibility, we also utilized the Alamar Blue assay, an indicator based on metabolic activity.[23] As evidenced by the reduced relative fluorescence intensity of Alamar Blue, the Gel-AgÅPs group exhibited a reduced live cell count, confirming the superior inhibitory effect of Gel-AgÅPs on bacterial viability. Intriguingly, the Gel-AgÅPs and LEV-treated groups exhibited comparable bactericidal efficacy (Figure 2B) but without statistical significance ($p > 0.05$).

We also investigated the impact of Gel-AgÅPs on biofilm formation and survival. Managing infections can be challenging due to the presence of biofilms, which are complex and self-secreting communities of bacteria embedded in the extracellular matrix.[24, 25] The crystal violet staining assay, which measures OD at 570 nm, was performed to compare the effects of Gel-AgÅPs and Gel-blank on biofilm formation. According to the results (Figure 2C), the Gel-AgÅPs exhibited significantly lower OD values, indicating a marked inhibition of biofilm formation by *E. coli*, *S. aureus*, and *P. aeruginosa*. Furthermore, there was a significant disruption of existing biofilms when Gel-AgÅPs were introduced at later stages of biofilm development (Figure 2D). Notably, Gel-AgÅPs exerted a more significant inhibitory effect on biofilm formation and survival than the Gel-blank.

These findings collectively suggest that Gel-AgÅPs have exceptional antibacterial potential and could serve as a highly effective antibacterial intervention in clinical settings, particularly in combating orthopedic implant-associated infections.

Efficacy of PEG hydrogel infused with AgÅPs in reducing bacterial colonization in infected femoral fractures

When treating long bone fractures (e.g., femurs), fixation devices are required to stabilize the injury, facilitate healing, and ensure mobility recovery. However, these devices are associated with complications, such as bacterial infections, which pose significant challenges, often leading to bone resorption, reactive bone formation, implant loosening, and, ultimately, device failure.[26] As previously reported, we developed an *in vivo* mouse model of orthopedic implant infection to simulate this clinical scenario.[17, 27]

To evaluate the efficacy of Gel-AgÅPs in a clinical setting, we speculated that its administration would not affect normal fracture healing, a critical criterion for its potential use in preventing bacterial infections. We tested this hypothesis by treating a few femoral fractures in mice with Gel-AgÅPs and left others untreated. Bacterial delivery was deliberately excluded in this phase of the experiment. At 3- and 6-week post-treatment, femora were removed and subjected to μCT and histological analyses. Tissue and cartilage morphology were assessed through H/E and SO/FG staining. On the other hand, osteogenic and osteoclastic activities were evaluated through immunohistochemical staining for OCN and TRAP staining, respectively. As revealed by μCT reconstructions (Figure A1), there were no significant differences in the morphology and volume of the fracture callus at 3 weeks. Furthermore, these findings were supported by the histological assessments of H/E and SO/FG (Figure A2). Similarly, no differences were found in immunohistochemical OCN staining and TRAP staining of repaired femora between the untreated and Gel-AgÅPs-treated mice (Figure A3). Quantitative results also revealed no statistically significant differences ($p > 0.05$) (Figure A3). The fractures were almost completely healed after 6 weeks, with no discernible differences in callus volume between the untreated and Gel-AgÅPs-treated groups ($p > 0.05$, Figure A1E-H).

Subsequently, we assessed Gel-AgÅPs' capability to prevent *E. coli* infection *in vivo* using the infected femur fracture model. Bacteria were combined with hydrogel components and polymerized *in situ* over the fracture in infected mice. Fractured femora were treated with *E. coli*-containing hydrogels and then polymerized *in situ* with or without AgÅPs. A group treated with soluble AgÅPs and an LEV (100 mg/kg) prophylaxis group were included for comparison. The animals were euthanized after 7 days, and viable bacterial levels were examined in the surrounding femur tissue, muscle, and stabilization needle (Figure 3A). The Gel-blank-treated infected controls exhibited high bacterial colony counts, indicating persistent infection (Figure 3A and B). Consistent with clinical observations, the prophylactic LEV treatment group showed elevated bacteria levels (Figure 3A and B), highlighting the limitations of systemic antibiotic regimens in eliminating *E. coli* infections.[28] On the other hand, the Gel-AgÅPs treatment group exhibited significantly lower bacterial colonization compared to the

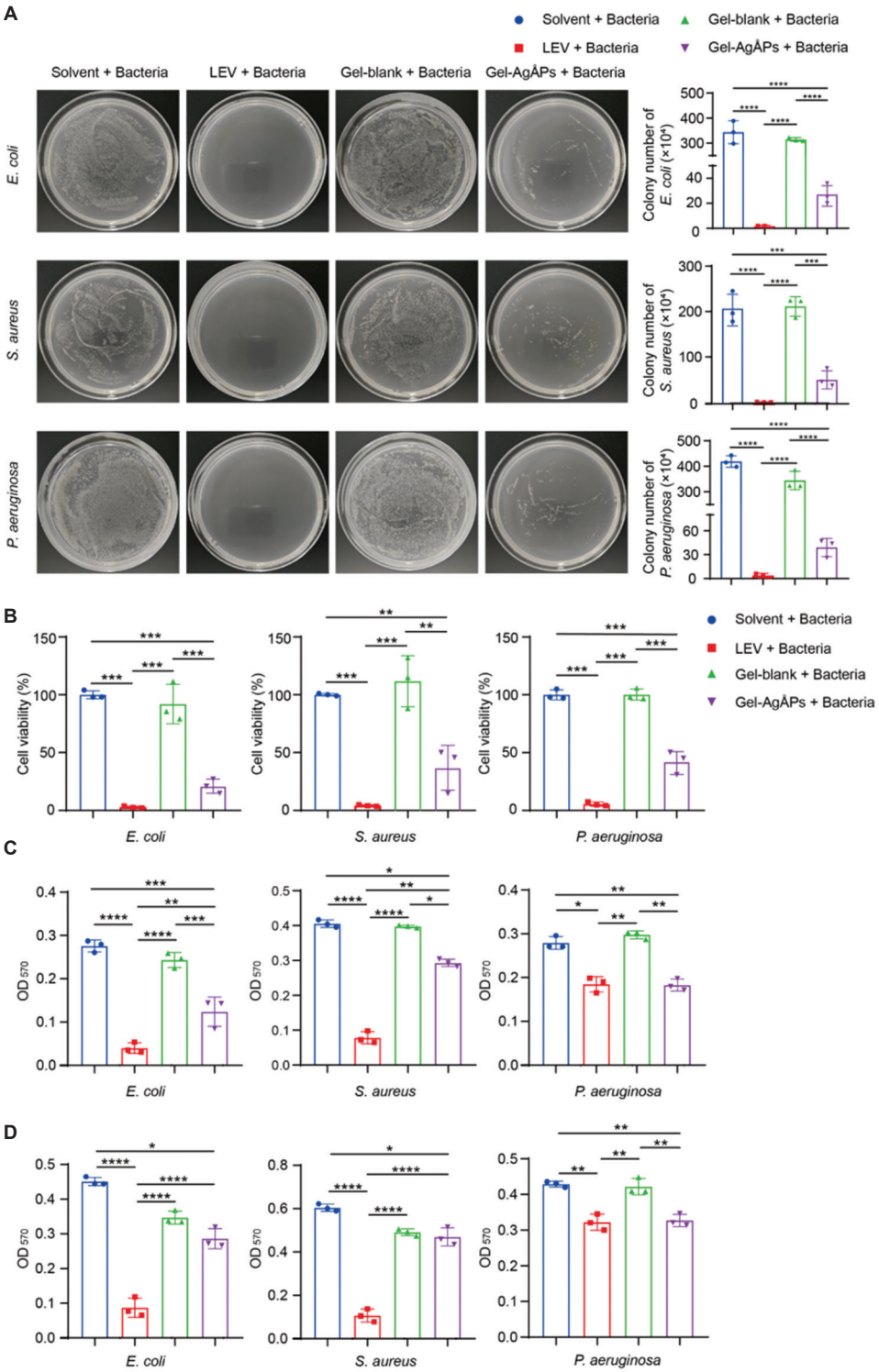

Figure 2. Antibacterial efficacy of polyethylene glycol hydrogel infused with AgÅPs against common bacteria. (A) Digital photos of bacterial colonies on agar plates from different treatment groups, with corresponding colony count quantification. n = 3 per group. (B) Alamar Blue assay for cell viability of bacteria treated with LEV, Gel-blank, and Gel-AgÅPs for 4 h. n = 3 per group. (C) Optical density measurements of crystal violet-stained biofilms formed by bacteria in various treatment groups. n = 3 per group. (D) The optical density of crystal violet-stained residual biofilms after exposure to different treatments. n = 3 per group.

Note: Statistical significance determined at $*p < 0.05$, $**p < 0.01$, $***p < 0.001$, and $****p < 0.0001$.

Abbreviations: AgÅPs: Ångstrom-scale silver particles; CFU: Colony-forming units. *E. coli: Escherichia coli*; Gel: Hydrogel; LEV: Levofloxacin; OD: Optical density; *P. aeruginosa: Pseudomonas aeruginosa; S. aureus: Staphylococcus aureus.*

infection-only control group (Figure 3A and B). Soluble AgÅPs had varying efficacy in reducing bacterial colony counts. They were also found to be inferior to both the LEV and Gel-AgÅPs treatment groups (Figure 3A and B), highlighting the effectiveness of hydrogel delivery systems in infection management. Notably, although LEV prophylaxis treatment

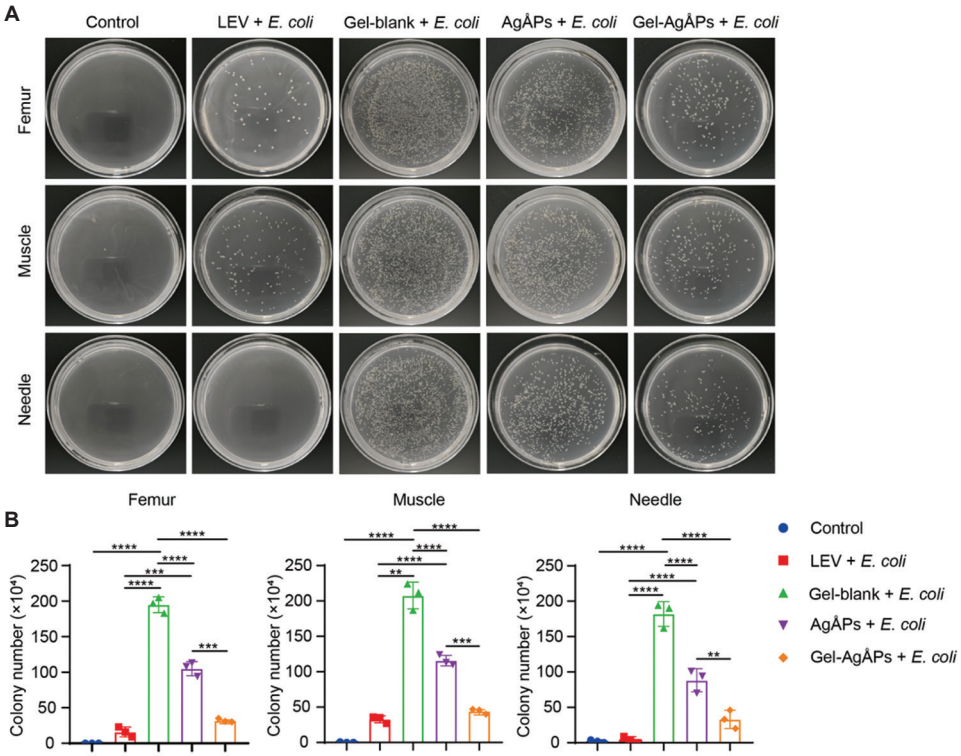

Figure 3. Efficacy of polyethylene glycol hydrogel infused with AgÅPs in reducing bacterial colonization in infected femoral fractures. Digital photos of bacterial colonies recovered from the femur surface, (A) surrounding muscle tissue, and stabilization needle after 7 days, with (B) corresponding colony count quantification across different treatment groups. n = 3 per group.
Note: Statistical significance determined at $^{**}p < 0.01$, $^{***}p < 0.001$, and $^{****}p < 0.0001$.
Abbreviations: AgÅPs: Ångstrom-scale silver particles; *E. coli: Escherichia coli*; Gel: Hydrogel; LEV: Levofloxacin.

outperformed Gel-AgÅPs treatment in terms of bactericidal efficacy, the difference was not statistically significant ($p > 0.05$, Figure 3B). This implies that the topical application of Gel-AgÅPs could be a viable alternative to antibiotics, particularly in cases of antibiotic resistance or complications due to systemic antibiotic use-induced liver and kidney damage.

Overall, these findings suggest that Gel-AgÅPs effectively eliminated bacterial infections in bone fractures, outperforming the direct delivery of soluble AgÅPs, thereby presenting a promising alternative to conventional antibiotic therapies.

Therapeutic effectiveness of PEG hydrogel infused with AgÅPs in the healing of infected femoral fractures

In a mouse femoral fracture model, we conducted a comprehensive assessment of functional fracture healing at 3- and 6-week post-infection to determine whether Gel-AgÅPs can alleviate bacterial infection and accelerate fracture repair. After inducing fractures, the mice were infected with *E. coli* and treated with Gel-AgÅPs or Gel-blank (control). In addition, a control group with an intact immune response was included as a benchmark for positive healing. Each group's BV/TV was analyzed to quantitatively evaluate the extent of new bone tissue formation.

The μCT reconstructions revealed a significant difference in healing progress after 3 weeks of treatment (Figure 4A). The *E. coli*-infected Gel-blank group showed no callus formation but exhibited evidence of bone resorption and reactive bone formation, both of which are indicative of osteomyelitis. On the other hand, the sterile control group exhibited robust fracture callus development, as well as evidence of bone remodeling, indicating ongoing fracture healing. Notably, as evidenced by the formation of fracture calluses and a higher BV/TV ratio compared to the *E. coli*-infected Gel-blank group (39.60 ± 11.66%, n = 8), all animals in the Gel-AgÅPs-treated group (57.71 ± 8.45%, n = 7) showed significant progress in fracture healing ($p < 0.05$, Figure 4B-D).

At 6 weeks post-treatment, μCT reconstructions of the Gel-AgÅPs-treated group revealed near-complete healing of the fracture site. In contrast, the infected Gel-blank group showed persistent fracture lines and minimal callus formation (Figure 4E). Quantitatively, the Gel-AgÅPs group (77.33 ± 11.22%, n = 8) had a significantly higher BV/TV ratio than the infection group (47.31 ± 14.95%, n = 9) ($p < 0.05$). Notably, no significant differences were found in BV, TV, or BV/TV ratio between untreated and Gel-AgÅPs-treated mice ($p > 0.05$, Figure 4F-H), indicating the hydrogel's non-inhibitory effect on bone healing.

A three-point bending test was performed to assess the biomechanical integrity of the fractured femur. We performed five independent replicate experiments, with each replicate containing a single fracture site. The consistency of our findings across the five independent samples provides a reasonable basis for our conclusions. The Gel-AgÅPs-treated infected fractures had a higher biomechanical strength

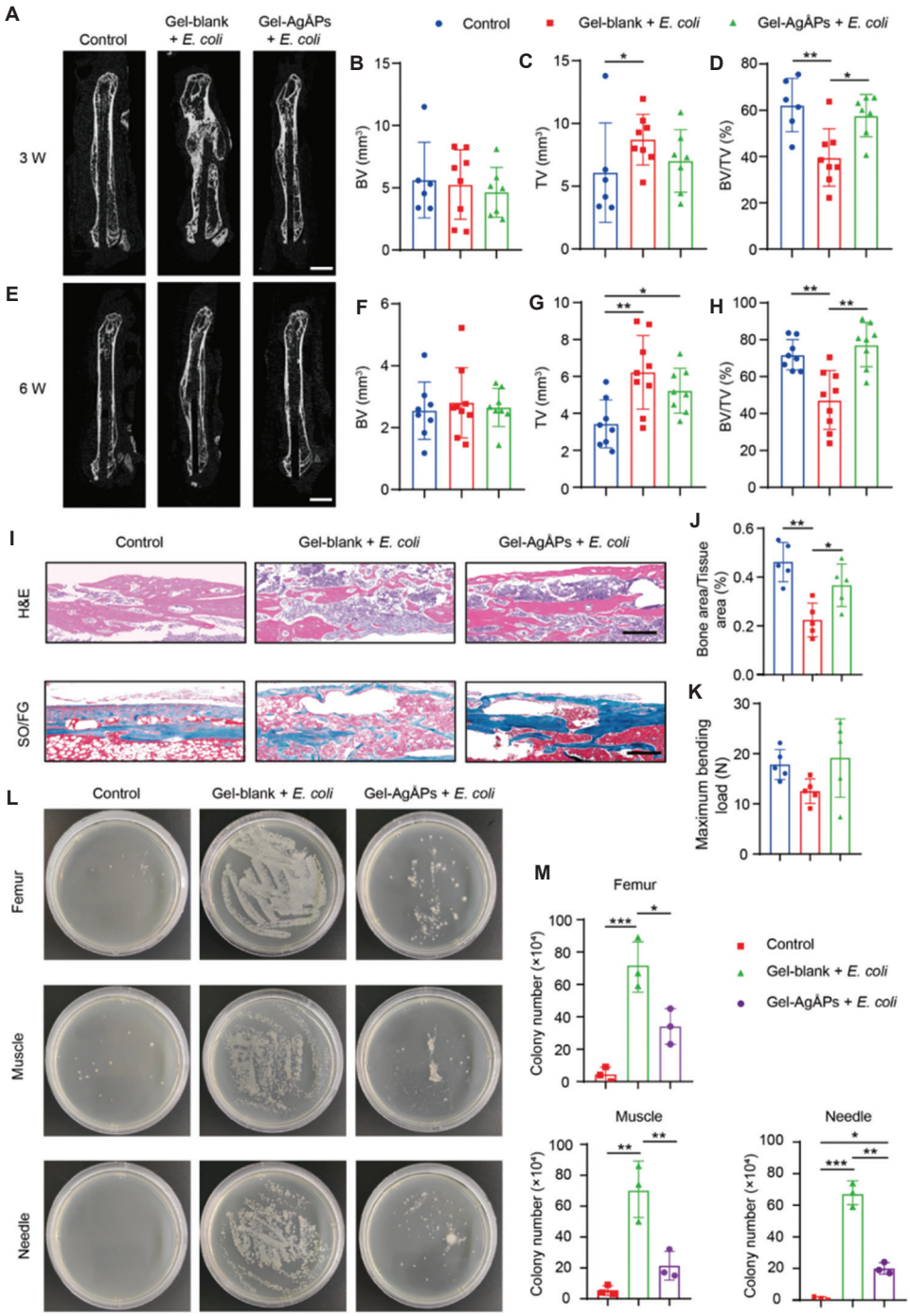

Figure 4. Therapeutic effectiveness of polyethylene glycol hydrogel infused with AgÅPs in the healing of infected femoral fractures. (A) Representative micro-computed tomography images of fractured femora from different treatment groups at 3 weeks. Scale bar: 5 mm, magnification: 2×. Quantitative analyses of (B) BV, (C) TV, and (D) BV/TV ratio at 3 weeks. Control: n = 6, Gel-blank + *E. coli*: n = 8, Gel-AgÅPs + *E. coli*: n = 7. (E) Representative micro-computed tomography images at 6 weeks post-treatment. Scale bar: 5 mm, magnification: 2×. Quantitative analyses of (F) BV, (G) TV, and (H) BV/TV ratio at 6 weeks. Control: n = 8, Gel-blank + *E. coli*: n = 9, Gel-AgÅPs + *E. coli*: n = 8. Representative images of (I) H/E and SO/FG staining and (J) quantitative analysis of bone area/tissue area ratio at the fracture site. Scale bar: 250 μm, magnification: 10×, n = 5 per group. (K) Three-point bending test results for femoral ultimate load at 6 weeks. n = 5 per group. Digital photos of bacterial colonies recovered respectively from the femur surface, (L) surrounding muscle tissue, and stabilization needle at 3 weeks and (M) corresponding colony counts across treatment groups. n = 3 per group.
Note: Statistical significance determined at $*p < 0.05$, $**p < 0.01$, and $***p < 0.001$.
Abbreviations: AgÅPs: Ångstrom-scale silver particles; BV: Bone volume; *E. coli: Escherichia coli*; Gel: Hydrogel; H/E: Hematoxylin and eosin; SO/FG: Safranin-O/Fast Green; TV: Tissue volume.

(19.13 ± 6.99 N, Figure 4K) than the infected Gel-blank group (12.53 ± 2.18 N, Figure 4K). These findings were comparable to the biomechanical properties of the sterile control group (17.83 ± 2.68 N, Figure 4K), indicating a Gel-AgÅPs

treatment-induced enhanced mineralization and structural integrity.

Histological analysis further supported these findings. Compared to sterile controls, sections of the Gel-AgÅPs-treated infected fractures showed no significant morphological differences (Figure 4I). As evidenced by poor collagen staining at the fracture site, SO/FG staining in the *E. coli*-infected Gel-blank group showed inhibited fracture repair. Gel-AgÅPs-treated samples exhibited normal collagen deposition, comparable to the control group (Figure 4J). In addition, bacterial colony counts at 3-week post-fracture confirmed the persistent infection in the untreated controls (Figure 4L and M). The Gel-AgÅPs-treated mice remained almost sterile (Figure 4L and M), confirming the results obtained 7-day post-surgery (Figure 3A and B).

In summary, these findings demonstrate that in addition to significantly reducing bacterial colonization in infected fractures, Gel-AgÅPs also supported effective and complete fracture repair, making them a promising therapeutic agent in the management of infected orthopedic injuries.

Establishment of an anti-inflammatory environment through PEG hydrogel infused with AgÅP application

At 3-week post-infection, we conducted a comprehensive analysis involving treatment with either Gel-AgÅPs or Gel-blank to assess the safety and efficacy of Gel-AgÅPs therapy in modulating inflammatory response. We employed immunohistochemical staining to analyze the presence and levels of inflammatory factors in tissue samples from fractures treated with *E. coli*-containing hydrogels, as well as with and without AgÅPs. We specifically focused on the levels of TNF-α and IL-1β, which are key cytokines in inflammatory responses to infections.[29] The *E. coli*-treated group exhibited higher levels of these cytokines compared to both the control and Gel-AgÅPs-treated groups (Figure 5A-D). Notably, no significant differences were observed in cytokine levels between the Gel-AgÅPs-treated and control groups (Figure 5A-D). These findings suggest that Gel-AgÅPs effectively restored the local inflammatory environment, providing compelling evidence that in addition to eradicating infectious bacteria, Gel-AgÅPs also facilitate the establishment of an inflammatory milieu conducive to fracture repair. *In vitro*, we stimulated BMSCs

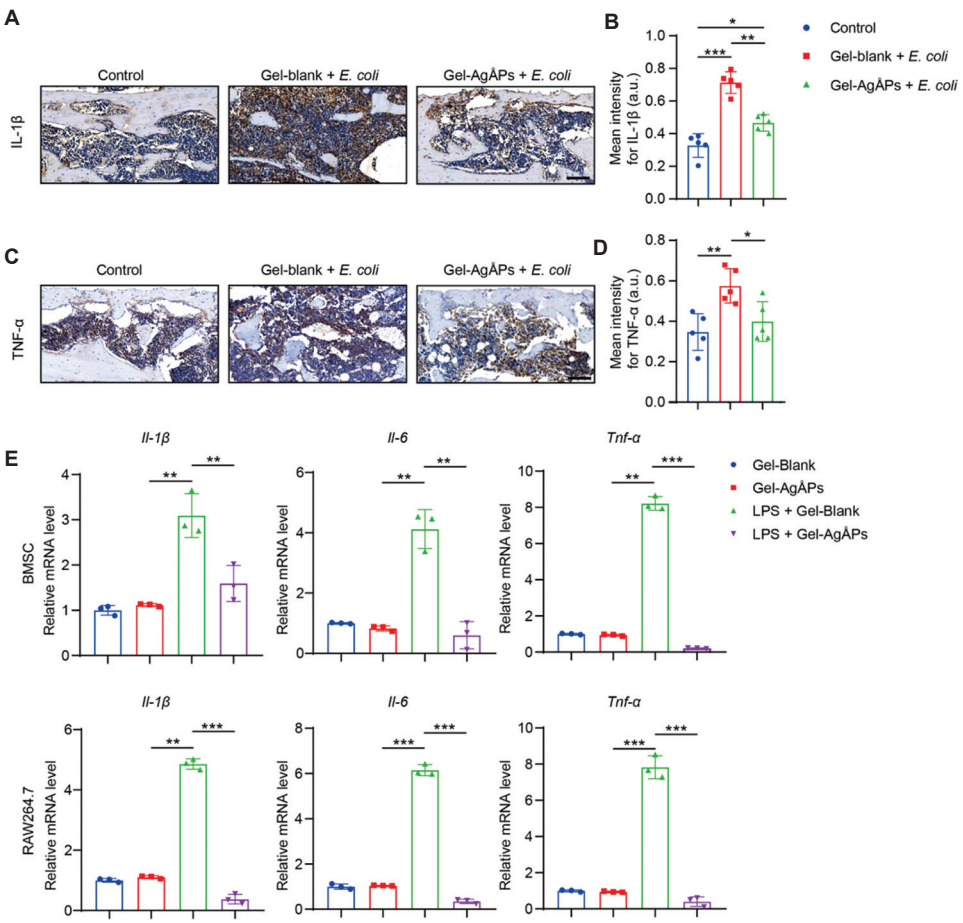

Figure 5. Establishment of an anti-inflammatory environment through polyethylene glycol hydrogel infused with AgÅPs application. Representative immunohistochemical staining images of (A) IL-1β and (C) TNF-α at the fracture site. Scale bar: 100 μm, magnification: 20×. Quantitative analysis of (B) IL-1β and (D) TNF-α intensity levels. n = 5 per group. (E) The expression level of inflammation-related genes (*Il1b*, *Il6*, and *Tnfa*) in BMSC and RAW264.7 cells stimulated by LPS, tested using qualitative real-time polymerase chain reaction. n = 3 per group.
Note: Statistical significance determined at $^{*}p < 0.05$, $^{**}p < 0.01$, and $^{***}p < 0.001$.
Abbreviations: AgÅPs: Ångstrom-scale silver particles; BMSC: Bone marrow mesenchymal stem cell; *E. coli: Escherichia coli*; Gel: Hydrogel; IL: Interleukin; LPS: Lipopolysaccharide; TNF: Tumor necrosis factor.

and RAW 264.7 cells with lipopolysaccharide (LPS) to simulate the excessive inflammatory state caused by bacterial infection and assess the expression levels of inflammatory factors (such as *Il1b*, *Il6*, and *Tnfa*). According to the results, Gel-AgÅPs effectively inhibited LPS-induced inflammation *in vitro* ($p < 0.05$, Figure 5E).

Inhibition of osteoclast activity by PEG hydrogel infused with AgÅPs s in infected fracture healing

To investigate the effect of Gel-AgÅPs on osteogenic and osteoclastic differentiation during the repair of infected fractures, we first stained the fracture sites in the *E. coli*-infected mouse model with OCN immunohistochemical labeling. Consistent with established literature,[15, 16] the *E. coli*-infected group showed lower osteogenic activity compared to the control group ($p < 0.05$, Figure 6A and B). Notably, compared to the *E. coli*-infected group, the Gel-AgÅPs-treated group did not show a significantly higher osteoblast intensity at the fracture site ($p > 0.05$, Figure 6A and B). Moreover, qRT-PCR analysis of osteoblastogenesis-related genes (*Bglap*, *Alpl*, and *Runx2*) showed that Gel-AgÅPs and Gel-blank had no significant difference in the osteoblast formation of BMSCs ($p > 0.05$, Figure 6E). This finding suggests that the beneficial impact of Gel-AgÅPs on infected fracture healing is not associated with enhanced osteoblast differentiation.

We then conducted TRAP histochemical staining at the fracture site to assess osteoclastic activity. Further analysis of the TRAP staining results revealed that the Gel-AgÅPs-treated group had significantly lower numbers of osteoclast on the trabecular surface at the fracture site compared to the *E. coli*-only group (Figure 6C and D), indicating that Gel-AgÅPs effectively suppressed osteoclast differentiation. Notably, the *in vitro* assays revealed that Gel-AgÅPs had a greater ability than Gel-blank to inhibit osteoclast formation of RAW

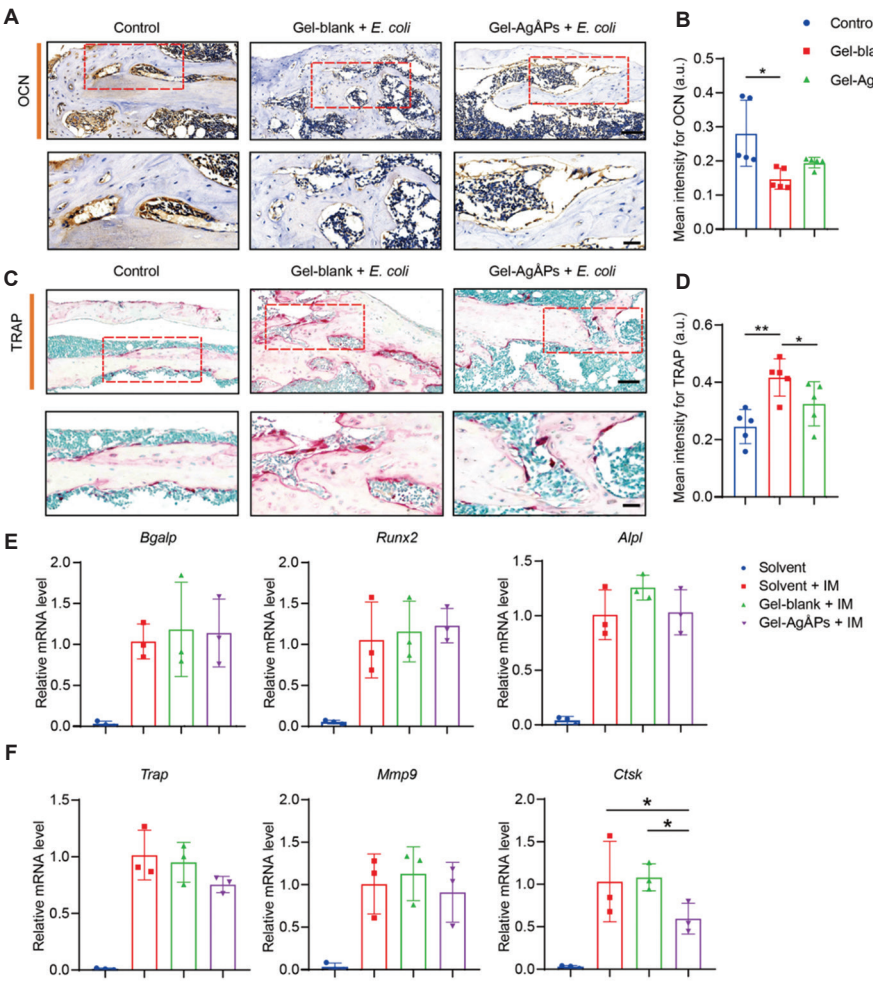

Figure 6. Inhibition of osteoclast activity by polyethylene glycol hydrogel infused with AgÅPs in infected fracture healing. (A) Representative OCN immunohistochemical staining at the fracture site, with (B) quantitative analysis of OCN intensity. The red rectangular boxes indicate the magnified area shown below. Scale bars: 50 μm or 25 μm (zoomed), magnification: 10× (upper), 20× (lower). n = 5 per group. (C) Representative TRAP staining images and (D) quantitative analysis of positively stained areas at the fracture site. The red rectangular boxes indicate the magnified area shown below. Scale bars: 100 μm or 50 μm (zoomed), magnification: 20× (upper), 40× (lower). n = 5 per group. Qualitative real-time polymerase chain reaction analysis of the expression of (E) osteoblastogenesis-related genes, including *Bglap*, *Runx2,* and *Alpl*, and (F) osteoclastogenesis-related genes, including *Trap*, *Mmp9,* and *Ctsk*. n = 3 per group.

Note: Statistical significance determined at $*p < 0.05$ and $**p < 0.01$.

Abbreviations: AgÅPs: Ångstrom-scale silver particles; *E. coli: Escherichia coli*; Gel: Hydrogel; IM: Induced medium; OCN: Osteocalcin; TRAP: Tartrate resistant acid phosphatase.

264.7, as revealed by qRT-PCR analysis of the expression of osteoclastogenesis-related genes (*Trap*, *Mmp9*, and *Ctsk*, Figure 6F). These findings implied the predominance of inflammatory and immune responses in bacterial infection at the fracture site. The infection-induced excessive inflammatory response promotes osteoclast precursor cell fusion, enhancing bone resorption and thereby delaying fracture healing.

Biocompatibility and safety profiles of PEG hydrogel infused with Ångstrom-scale silver particles *in vitro*

We induced BMSCs to differentiate toward an osteogenic lineage in the presence of Gel-AgÅPs. According to the results, Gel-AgÅPs did not impede BMSC osteogenic differentiation, as determined by assessments of calcium deposition (Figure 7A and B) and alkaline phosphatase activity (Figure 7C). This finding suggests that while Gel-AgÅPs effectively eradicated *E. coli*, they do not interfere with BMSC osteogenic differentiation. In addition, TRAP staining of osteoclast-induced RAW264.7 cells revealed that Gel-AgÅPs had an inhibitory effect on osteoclast differentiation (Figure 7D and E), which is consistent with our *in vivo* experimental results. Then, we performed CCK-8 analysis to investigate the impact of AgÅPs on BMSC and RAW264.7 cell viability *in vitro*. CCK-8 assay revealed that AgÅPs had no significant toxicity on these cells (Figure A4A and B).

Biocompatibility and safety profiles of PEG hydrogel infused with AgÅPs *in vivo*

To explore potential systemic effects, we examined the long-term (6 weeks) effects of the topical application of Gel-AgÅPs in an infected fracture-induced mouse model. Serum analyses, including TNF-α, IFN-γ, IL-2, and IL-6 levels, revealed no significant changes in blood routine parameters following Gel-AgÅPs treatment (Figure 7F). Following Gel-AgÅPs application, H/E staining of the organs (lung, liver, spleen, kidney, and heart) revealed no abnormal changes (Figure 7G). These findings suggest that Gel-AgÅPs are well-tolerated at therapeutically effective doses, offering a favorable safety profile for use in infected fracture therapy.

Discussion

Infection of internal fixation in fractures is a serious clinical issue, and effective treatment methods are lacking. Current treatment options are limited to prolonged use of systemic antibiotics, surgical debridement, and removal of internal fixation implants, but they face challenges such as antibiotic resistance. We previously reported that intravenous administration of AgÅPs solution could effectively and broadly kill bacteria. AgÅPs achieve this by anchoring to and penetrating bacterial membranes, leading to membrane destruction and leakage of intracellular contents. In addition, AgÅPs disrupt critical intracellular processes, including protein denaturation and DNA replication.[13] However, due to potential systemic side effects and the lack of a suitable delivery vehicle, further exploration is needed for the local treatment of fracture internal fixation infections. Hence, we designed an injectable hydrogel to deliver AgÅPs, Gel-AgÅPs, to the infected fracture site, aiming to clear local infections and enhance fracture healing. Notably, our results suggest that the injectable hydrogel-loaded AgÅPs have dual functions: directly killing bacteria and reducing inflammation at the infection site. These actions aim to eradicate fracture internal fixation infections, inhibit inflammation-induced osteoclast differentiation, and ultimately accelerate the healing process of infected fractures.

Fracture healing involves three overlapping phases: inflammation, bone repair, and bone remodeling. The initial inflammatory phase sets the stage for bone repair and remodeling, ultimately leading to callus formation and mineralization.[30, 31] However, excessive inflammation has been shown to enhance osteoclast activity while inhibiting osteoblast activity, disrupting the critical balance between bone formation and resorption, which adversely affects fracture healing.[32-34] Our findings demonstrated that internal fixation-associated bone infections triggered the release of inflammatory markers and a robust inflammatory response characterized by elevated levels of IL-1β, IL-6, and TNF-α. The anti-inflammatory effect of Gel-AgÅPs is achieved through both direct and indirect mechanisms. First, the proliferation of bacteria is a primary trigger for the inflammatory cascade and the subsequent "cytokine storm." By eliminating bacteria at the infection site, Gel-AgÅPs indirectly suppresses inflammation by reducing the microbial burden and limiting the release of bacterial toxins and pro-inflammatory molecules. Second, we conducted *in vitro* studies to evaluate whether Gel-AgÅPs could directly inhibit inflammation independent of its antibacterial activity. The results revealed that Gel-AgÅPs significantly suppressed LPS-induced inflammation *in vitro*, highlighting its ability to directly modulate inflammatory pathways in host cells. Therefore, we hypothesized that the anti-inflammatory effects of Gel-AgÅPs are not solely due to infection alleviation but also involve a direct action on host cells to modulate the inflammatory response.

Specifically, Gel-AgÅPs eliminate bacterial colonization at the fracture site, restoring an inflammatory environment conducive to fracture healing. By mitigating inflammation-induced bone resorption, Gel-AgÅPs reestablish the balance between osteoblast and osteoclast activities, speeding up the recovery of infected fractures. The role of inflammation in regulating osteoblast and osteoclast activities is inherently complex and highly context-dependent. The coupling between osteoclasts and osteoblasts is crucial for bone remodeling, particularly during fracture repair. Infected fractures disrupt this delicate balance, resulting in excessive bone loss and compromised osteoblast function.[35-37] Our study demonstrated that Gel-AgÅPs significantly alleviated inflammation, which mitigated osteoclast overactivation and preserved the bone matrix. Interestingly, Gel-AgÅPs did not markedly enhance osteoblast differentiation. This observation can be attributed to their ability to restore a balanced microenvironment favorable for normal bone remodeling without overstimulating osteoblast activity. Furthermore, by suppressing osteoclast activity, Gel-AgÅPs may indirectly reduce the release of coupling factors such as TGF-β and IGF-1, which play a role in promoting osteoblast differentiation.[36, 37] Although our current data

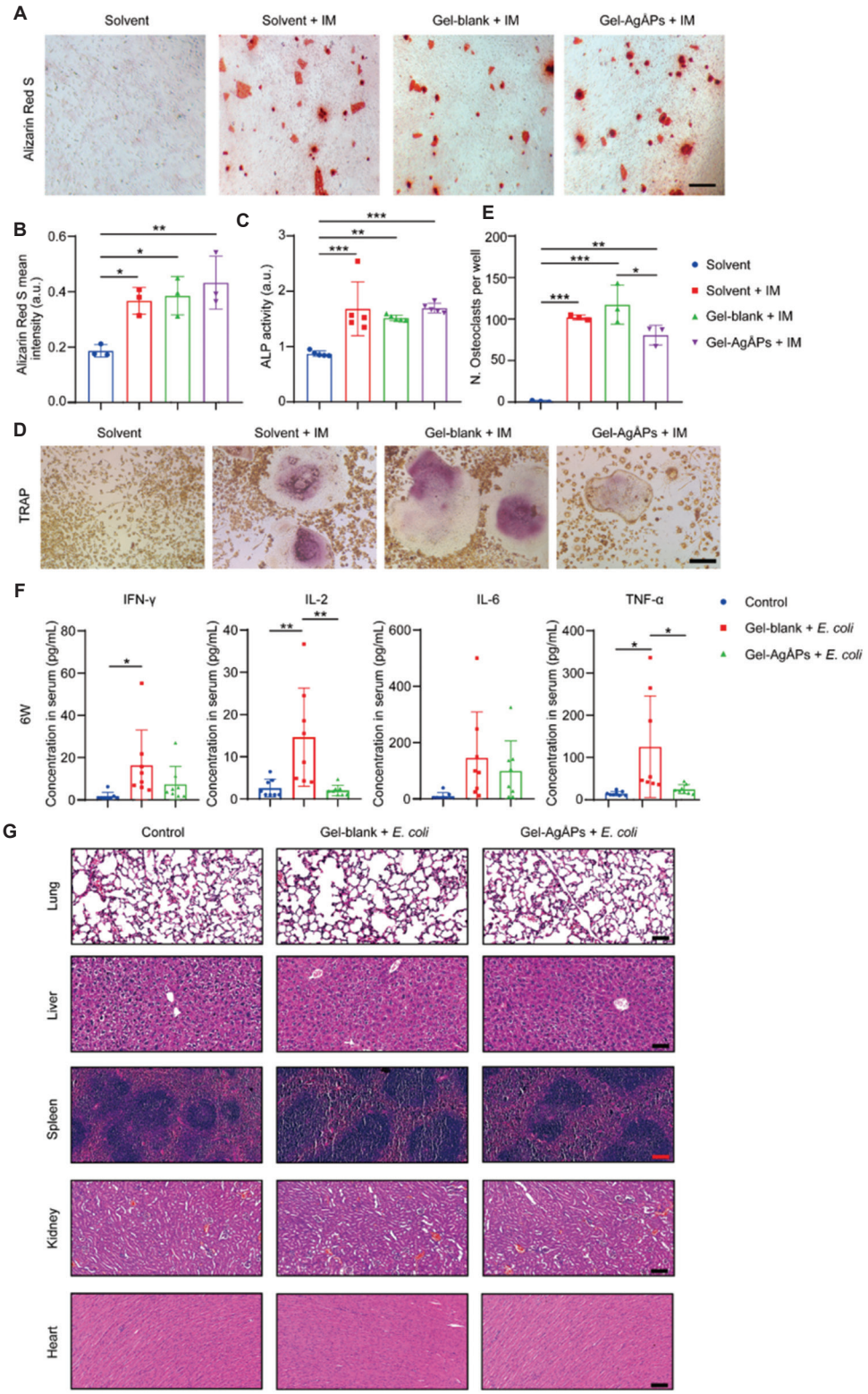

Figure 7. Assessment of biocompatibility and safety profiles of polyethylene glycol hydrogel infused with AgÅPs in orthopedic applications. (A) Representative images of Alizarin Red S staining of BMSC mineral deposition, with quantitative analyses of (B) mineralization intensity and (C) ALP activity. Scale bar: 200 μm, magnification: 10×, (B) n = 3 or (C) 5 per group. (D) Representative images of TRAP staining of RAW264.7 osteoclasts, with (E) quantification of osteoclast numbers. Scale bar: 100 μm, magnification: 20×, n = 3 per group. (F) Serum concentrations of IFN-γ, IL-2, IL-6, and TNF-α at 6 weeks. n = 8 per group. (G) Hematoxylin and eosin staining images of lung, liver, spleen, kidney and heart sections from mice after internal fixation of fractures from each treatment group. Scale bars, 100 μm (red) or 50 μm (black), magnification: 20×. n = 5 per group.

Note: Statistical significance determined at $^{*}p < 0.05$, $^{**}p < 0.01$, $^{***}p < 0.001$.

Abbreviations: AgÅPs: Ångstrom-scale silver particles; ALP: Alkaline phosphatase; *E. coli: Escherichia coli*; Gel: Hydrogel; IL: Interleukin; IFN: Interferon; IM: Induced medium; TNF: Tumor necrosis factor; TRAP: Tartrate resistant acid phosphatase.

does not indicate a direct impact of Gel-AgÅPs on osteoblast differentiation, it remains possible that osteoblast-related responses might emerge at other time points. Further studies are warranted to investigate this potential temporal effect and fully elucidate the role of Gel-AgÅPs in fracture repair.

Despite the promising findings, our study has several limitations. First, the lack of research on Gel-AgÅPs in large animal models limits the translational potential of this work for clinical application. Second, the effect of Gel-AgÅPs on the healing of infected fractures was not assessed at multiple time points, leaving temporal dynamics unexplored. Lastly, further investigations are needed to better understand how the material properties of Gel-AgÅPs affect its sustained release efficiency and antibacterial performance. In addition, a more comprehensive evaluation of its biological safety is required to support its potential use in clinical settings.

Conclusion

This study presents a pioneering approach in orthopedic implant infection management, employing four-arm PEG hydrogels loaded with AgÅPs to effectively combat bacterial infections and facilitate bone repair. Our findings highlight the potential of Gel-AgÅPs as a biomaterial for *in situ* anti-infection applications in orthopedic implants. Therefore, the clinical potential of Gel-AgÅPs needs to be further explored to fully exploit their therapeutic benefits.

Authors contributions

Conceptualization: HX, YZ and ZW; *Data curation:* JG and WD; *Investigation:* BC, JG, WD, YL, YY, ZH, and ZG; *Methodology:* SZ, XC, YW, YY, and YZ; *Project administration:* ZW; *Resources:* JG, WD, XC, and YW; *Supervision:* HX and ZW; *Writing-original draft:* JG, WD, and ZW; *Writing-review & editing:* HX and YZ. All authors reviewed and approved the final version of the manuscript.

Financial support

This work was supported by the National Natural Science Foundation of China (Grant no.: 82125023 and 82072504 to HX and grant no.: 82272562 to ZW), the Science and Technology Innovation Program of Hunan Province (Grant no.: 2023RC3075 to ZW), and the Hunan Province Natural Science Foundation of China (Grant no.: 2023JJ20096 to ZW and grant no.: 2023JJ30872 to WD).

Acknowledgement

None.

Conflicts of interest statement

The authors declare no conflicts of interest.

Ethics approval and consent to participate

Animal care and experimental procedures were approved by the Ethics Review Committee of Xiangya Hospital of Central South University (approval number: 202101007) in accordance with the Guidelines for the Ethical Review of Laboratory Animal Welfare People's Republic of China National Standard GB/T 35892-2018.

Consent for publication

Not applicable.

Availability of data

Not applicable.

References

1. Depypere, M.; Morgenstern, M.; Kuehl, R.; Senneville, E.; Moriarty, T. F.; Obremskey, W. T.; Zimmerli, W.; Trampuz, A.; Lagrou, K.; Metsemakers, W. J. Pathogenesis and management of fracture-related infection. *Clin Microbiol Infect.* **2020**, *26*, 572-578. doi: 10.1016/j.cmi.2019.08.00
2. Darouiche, R. O. Treatment of infections associated with surgical implants. *N Engl J Med.* **2004**, *350*, 1422-1429. doi: 10.1056/NEJMra035415
3. Moriarty, T. F.; Metsemakers, W. J.; Morgenstern, M.; Hofstee, M. I.; Vallejo, D. A.; Cassat, J. E.; Wildemann, B.; Depypere, M.; Schwarz, E. M.; Geoff Richards, R. Fracture-related infection. *Nat Rev Dis Primers.* **2022**, *8*, 67. doi: 10.1038/s41572-022-00396-0
4. Campoccia, D.; Montanaro, L.; Arciola, C. R. The significance of infection related to orthopedic devices and issues of antibiotic resistance. *Biomaterials.* **2006**, *27*, 2331-2339. doi: 10.1016/j.biomaterials.2005.11.044
5. Arciola, C. R.; Campoccia, D.; Montanaro, L. Implant infections: Adhesion, biofilm formation and immune evasion. *Nat Rev Microbiol.* **2018**, *16*, 397-409. doi: 10.1038/s41579-018-0019-y
6. Metsemakers, W. J.; Morgenstern, M.; Senneville, E.; Borens, O.; Govaert, G. A. M.; Onsea, J.; Depypere, M.; Geoff Richards, R.; Trampuz, A.; Verhofstad, M. H. J.; Kates, S. J.; Raschke, M.; McNally, M. A.; Obremskey, W. T.; Fracture-Related Infection (FRI) Group. General treatment principles for fracture-related infection: Recommendations from an international expert group. *Arch Orthop Trauma Surg.* **2020**, *140*, 1013-1027. doi: 10.1007/s00402-019-03287-4
7. Iliaens, J.; Onsea, J.; Hoekstra, H.; Nijs, S.; Peetermans, W. E.; Metsemakers, W. J. Fracture-related infection in long bone fractures: A comprehensive analysis of the economic impact and influence on quality of life. *Injury.* **2021**, *52*, 3344-3349. doi: 10.1016/j.injury.2021.08.023
8. Holmes, A. H.; Moore, L. S.; Sundsfjord, A.; Steinbakk, M.; Regmi, S.; Karkey, A.; Guerin, P. J.; Piddock, L. J. V. Understanding the mechanisms and drivers of antimicrobial resistance. *Lancet.* **2016**, *387*, 176-187. doi: 10.1016/S0140-6736(15)00473-0
9. Jiang, N.; Wu, H. T.; Lin, Q. R.; Hu, Y. J.; Yu, B. Health care costs of post-traumatic osteomyelitis in China: Current situation and influencing factors. *J Surg Res.* **2020**, *247*, 356-363. doi: 10.1016/j.jss.2019.10.008
10. Pelgrift, R. Y.; Friedman, A. J. Nanotechnology as a therapeutic tool to combat microbial resistance. *Adv Drug Deliv Rev.* **2013**, *65*, 1803-1815. doi: 10.1016/j.addr.2013.07.011
11. Wu, Z.; Chan, B.; Low, J.; Chu, J. J. H.; Hey, H. W. D.; Tay, A. Microbial resistance to nanotechnologies: An important but understudied consideration using antimicrobial nanotechnologies in orthopaedic implants. *Bioact Mater.* **2022**, *16*, 249-270. doi: 10.1016/j.bioactmat.2022.02.014
12. Brennan, S. A.; Ní, F. C.; Devitt, B. M.; O'Mahony, F. J.; Brabazon, D.; Walsh, A. Silver nanoparticles and their orthopaedic applications. *Bone Joint J.* **2015**, *97-b*, 582-589. doi: 10.1302/0301-620X.97B5.33336
13. Xu, L.; Wang, Y. Y.; Huang, J.; Chen, C.Y.; Wang, Z. X.; Xie, H. Silver nanoparticles: Synthesis, medical applications and biosafety. *Theranostics.* **2020**, *10*, 8996-9031. doi: 10.7150/thno.45413
14. Wang, Z. X.; Chen, C. Y.; Wang, Y.; Li, F. X. Z.; Huang, J.; Luo, Z. W.; Rao, S. S.; Tan, S. Y.; Liu, Y. W.; Yin, H.; Wang, Y. Y.; He, Z. H.; Xia, K.; Wu, B.; Hu, H. K.; Luo, M. J.;... &. Xie, H. Angstrom-scale silver particles as a promising agent for low-toxicity broad-spectrum potent anticancer therapy. *Adv Funct Mater.* **2019**, *29*, 1808556. doi: 10.1002/adfm.201808556
15. Chen, C. Y.; Yin, H.; Chen, X.; Chen, T. H.; Liu, H. M.; Rao, S. S.; Tan, Y. J.; Qian, Y. X.; Liu, Y. W.; Hu, X. K.; Luo, M. J.; Wang, Z. X.; Liu, Z. Z.; Cao, J.; He, Z. H. Ångstrom-scale silver particle-embedded carbomer gel promotes wound healing by inhibiting bacterial colonization and inflammation. *Sci Adv.* **2020**, *6*, eaba0942. doi: 10.1126/sciadv.aba0942
16. Yin, H.; Zhou, M.; Chen, X.; Wan, T. F.; Jin, L.; Rao, S. S.; Tan, Y. J.; Duan, R. J.; Zhang, Y.; Wang, Z. X.; Wang, Y. Y.; He, Z. H. Fructose-coated Ångstrom silver prevents sepsis by killing bacteria and attenuating

bacterial toxin-induced injuries. *Theranostics*. **2021**, *11*, 8152-8171.
doi: 10.7150/thno.55334

17. Gong, J. S.; Zhu, G. Q.; Zhang, Y.; Chen, B.; Liu, Y. W.; Li, H. M.; He, Z. H.; Zou, J. T.; Qian, Y. X.; Zhu, S.; Hu, X. Y.; Rao, S. S.; Cao, J.; Xie, H.; Wang, Z. X.; Du, W. Aptamer-functionalized hydrogels promote bone healing by selectively recruiting endogenous bone marrow mesenchymal stem cells. *Mater Today Bio*. **2023**, *23*, 100854.
doi: 10.1016/j.mtbio.2023.100854
18. Deng, Y. Q.; Wang, Z. X.; Liu, X.; Wang, Y. Y.; Chen, Q.; Li, Z. L.; Bai Song Zheng 5, Zheng, B. S.; Ye, Q.; Gong, J. S.; Gong, J. S.; Zhu, G. Q.; Cao, T. S.; Cao, T. S. Ångstrom-scale silver particles potently combat SARS-CoV-2 infection by suppressing the ACE2 expression and inflammatory responses. *J Mater Chem B*. **2022**, *10*, 5454-5464.
doi: 10.1039/d2tb00336h
19. Kuang, X.; Wang, Z.; Luo, Z.; He, Z.; Liang, L.; Gao, Q.; Li, Y.; Xia, K.; Xie, Z.; Chang, R.; Wang, Y.; Liu, Y.; Zhao, S.; Su, J.; Wang, Y.; Situ, W.;... &. Liu, H. Ag nanoparticles enhance immune checkpoint blockade efficacy by promoting of immune surveillance in melanoma. *J Colloid Interface Sci*. **2022**, *616*, 189-200.
doi: 10.1016/j.jcis.2022.02.050
20. Yu, J. J.; Chen, F.; Wang, X. C.; Dong, N. G.; Lu, C. F.; Yang, G. C.; Chen, Z. Synthesis and characterization of MMP degradable and maleimide cross-linked PEG hydrogels for tissue engineering scaffolds. *Polym Degrad Stabil*. **2016**, *133*, 312-320.
doi: 10.1016/j.polymdegradstab.2016.09.008
21. Zhao, Y.; Wang, D. D.; Qian, T. W.; Zhang, J. M.; Li, Z. H.; Gong, Q. Y.; Ren, X.; Zhao, Y. Biomimetic nanozyme-decorated hydrogels with H (2) O(2)-activated oxygenation for modulating immune microenvironment in diabetic wound. *ACS Nano*. **2023,** *17*, 16854-16869.
doi: 10.1021/acsnano.3c03761
22. Cyphert, E. L.; Zhang, N.; Learn, G. D.; Hernandez, C. J.; von Recum, H. A. Recent advances in the evaluation of antimicrobial materials for resolution of orthopedic implant-associated infections *in vivo*. *ACS Infect Dis*. **2021**, *7*, 3125-3160.
doi: 10.1021/acsinfecdis.1c00465
23. Rampersad, S. N. Multiple applications of Alamar Blue as an indicator of metabolic function and cellular health in cell viability bioassays. *Sensors (Basel)*. **2012**, *12*, 12347-12360.
doi: 10.3390/s120912347
24. Li, P.; Gao, Z.; Tan, Z.; Xiao, J.; Wei, L.; Chen, Y. New developments in anti-biofilm intervention towards effective management of orthopedic device related infections (ODRI's). *Biofouling*. **2021**, *37*, 1-35.
doi: 10.1080/08927014.2020.1869725
25. Sharma, S.; Mohler, J.; Mahajan, S. D.; Schwartz, S. A.; Bruggemann, L.; Aalinkeel, R. Microbial biofilm: A review on formation, infection, antibiotic resistance, control measures, and innovative treatment. *Microorganisms*. **2023**, *11*, 1614.
doi: 10.3390/microorganisms11061614
26. Metsemakers, W. J.; Morgenstern, M.; McNally, M. A.; Moriarty, T. F.; McFadyen, I.; Scarborough, M.; Athanasou, N. A.; Ochsner, P. E.; Kuehl, R.; Raschke, M.; Borens, O.; Xie, Z.; Velkes, S.; Hungerer, S.; Kates, S. L. Fracture-related infection: A consensus on definition from an international expert group. *Injury*. **2018**, *49*, 505-510.
doi: 10.1016/j.injury.2017.08.040
27. Ambrosi, T. H.; Marecic, O.; McArdle, A.; Sinha, R.; Gulati, G. S., Tong, X.; Wang, Y.; Steininger, H. M.; Hoover, M. Y.; Koepke, L. S.; Murphy, M. P.; Sokol, S.,...&. Chan, C. K. F. Aged skeletal stem cells generate an inflammatory degenerative niche. *Nature*. **2021**, *597*, 256-262.
doi: 10.1038/s41586-021-03795-7
28. Steinmetz, S.; Wernly, D.; Moerenhout, K.; Trampuz, A.; Borens, O. Infection after fracture fixation. *EFORT Open Rev*. **2019**, *4*, 468-475.
doi: 10.1302/2058-5241.4.180093
29. Medzhitov, R. The spectrum of inflammatory responses. *Science*. **2021**, *374*, 1070-1075.
doi: 10.1126/science.abi5200
30. Claes, L.; Recknagel, S.; Ignatius, A. Fracture healing under healthy and inflammatory conditions. *Nat Rev Rheumatol*. **2012**, *8*, 133-143.
doi: 10.1038/nrrheum.2012.1
31. Masters, E. A.; Ricciardi, B. F.; Bentley, K. L. M.; Moriarty, T. F.; Schwarz, E. M.; Muthukrishnan, G. Skeletal infections: Microbial pathogenesis, immunity and clinical management. *Nat Rev Microbiol*. **2022**, *20*, 385-400.
doi: 10.1038/s41579-022-00686-0
32. Yang, Y.; Li M.; Zhou, B.; Jiang, X.; Zhang, D.; Luo, H. Graphene oxide/gallium nanoderivative as a multifunctional modulator of osteoblastogenesis and osteoclastogenesis for the synergistic therapy of implant-related bone infection. *Bioact Mater*. **2023**, *25*, 594-614.
doi: 10.1016/j.bioactmat.2022.07.015
33. Ma, L.; Cheng, Y.; Feng, X.; Zhang, X.; Lei, J.; Wang, H.;; Xu, Y.; Tong, B.; Zhu, D.; Wu, D.; Zhou, X.; Liang, H.; Zhao, K.; Wang, K.; Tan, L.; Zhao, Y.; Yang, C. A Janus-ROS healing system promoting infectious bone regeneration via sono-epigenetic modulation. *Adv Mater*. **2024**, *36*, e2307846.
doi: 10.1002/adma.202307846
34. Takayanagi, H. Osteoimmunology: Shared mechanisms and crosstalk between the immune and bone systems. *Nat Rev Immunol*. **2007**, *7*,292-304.
doi: 10.1038/nri2062
35. Wang, Z. X.; Lin, X.; Cao, J.; Liu, Y. W.; Luo, Z. W.; Rao, S. S.; Wang, Q.; Wang, Y. Y.; Chen, C. Y.; Zhu, G. Q.; Li, F. X. Z.; Tan, Y. J.; Hu, Y.; Yin, H.; Li, Y. Y.;... &. Xie, H. Young osteocyte-derived extracellular vesicles facilitate osteogenesis by transferring tropomyosin-1. *J Nanobiotechnology*. **2024**, *22*, 208.
doi: 10.1186/s12951-024-02367-x
36. Tang, Y.; Wu, X. W.; Lei, W. Q., Pang, L. J.; Wan, C.; Shi, Z., Zhao, L.; Nagy, T. R.; Peng, X.; Hu, J.; Feng, X.; Hul, W. V.; Wan, M.; Cao, X. TGF-beta1-induced migration of bone mesenchymal stem cells couples bone resorption with formation. *Nat Med*. **2009**, *15*, 757-765.
doi: 10.1038/nm.1979
37. Xian, L. L.; Wu, X. W.;Pang, L. J.; Lou, M.; Rosen, C. J.; Qiu, T.; Crane, J.; Frassica, F.; Zhang, L.; Pablo Rodriguez, J.; Jia, X.; Yakar, S.; Xuan, S.; Efstratiadis, A.; Wan, M.; Cao, X. Matrix IGF-1 maintains bone mass by activation of mTOR in mesenchymal stem cells. *Nat Med*. **2012,** *18*, 1095-1101.
doi: 10.1038/nm.2793

Received: December 8, 2024
Revised: January 15, 2025
Accepted: February 28, 2025
Available online: March 25, 2025

Appendix files

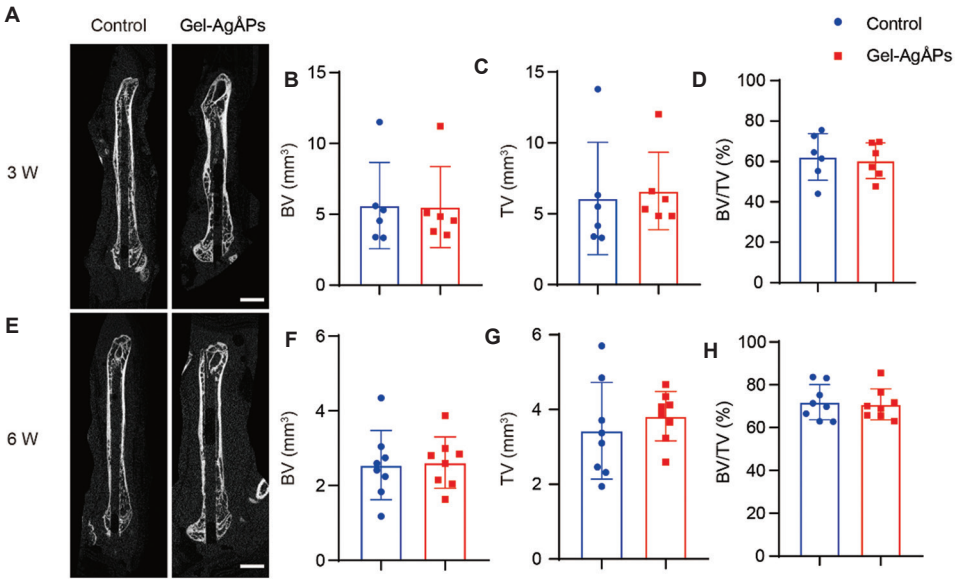

Figure A1. Polyethylene glycol hydrogel infused with AgÅPs supports fracture healing. (A) Representative micro-computed tomography (μCT) images showing fractured femora in various treatment groups at 3 weeks post-injury. Scale bar: 5 mm, magnification: 2×. Quantitative analysis of (B) BV, (C) TV, and (D) the ratio of BV/TV at 3 weeks post-treatment. n = 6 per group. (E) Representative μCT images at 6 weeks post-treatment. Scale bar: 5 mm, magnification: 2×. Quantitative evaluation of (F) BV, (G) TV, and (H) BV/TV ratio at 6 weeks post-treatment. n = 8 per group.
Abbreviations: AgÅPs: Ångstrom-scale silver particles; BV: Bone volume; TV: Tissue volume.

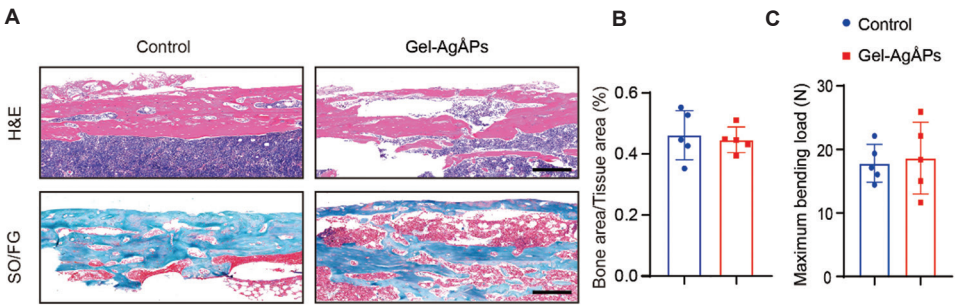

Figure A2. Histological assessment of fracture healing. (A) Representative images of H/E and SO/FG staining with corresponding (B) quantitative analyses of the positively stained areas at the fracture site. Scale bar: 250 μm, magnification: 10×, n = 5 per group. (C) Three-point bending tests measuring the ultimate load of femoral fractures at 6 weeks post-treatment. n = 5 per group.
Abbreviations: AgÅPs: Ångstrom-scale silver particles; H/E: Hematoxylin and eosin; SO/FG: Safranin-O/Fast Green.

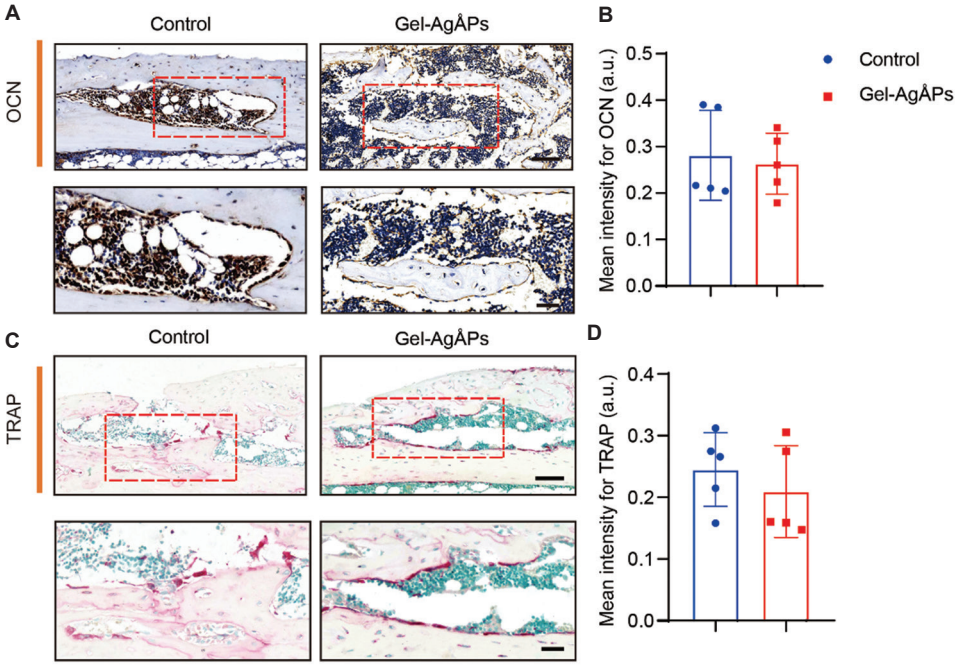

Figure A3. Immunohistochemical evaluation of osteogenic and osteoclastic activity. (A) Representative immunohistochemical staining for OCN at the fracture site and (B) quantitative analysis of OCN intensity. Scale bars: 50 μm, or 25 μm (zoomed), magnification: 10× (upper), 20× (lower). n = 5 per group. (C) Representative TRAP staining of the fracture area with (D) quantitative analysis of the positively stained area for osteoclast activity. Scale bars: 100 μm or 50 μm (zoomed), magnification: 20× (upper), 40× (lower). n = 5 per group.
Abbreviations: AgÅPs: Ångstrom-scale silver particles; OCN: Osteocalcin; TRAP: Tartrate resistant acid phosphatase.

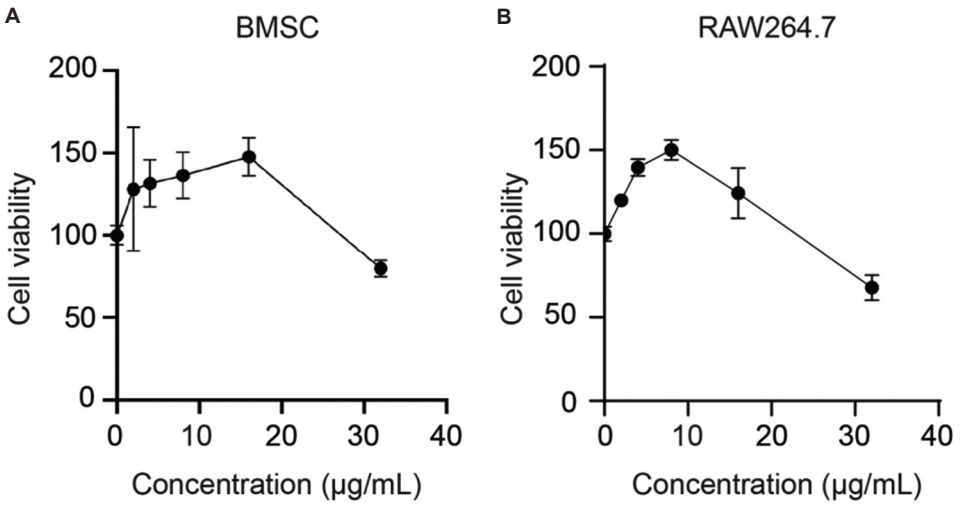

Figure A4. Effects of Ångstrom-scale silver particles on cell viability. Cell counting kit-8 assay of AgÅPs in (A) BMSC and (B) RAW264.7 cells.
Abbreviation: BMSC: Bone marrow mesenchymal stem cell.